NANO LETTERS
Text
Letter
pubs.acs.org/NanoLett

Engineered Micro- and Nanoscale Diamonds as Mobile Probes for High-Resolution Sensing in Fluid

Paolo Andrich,[†,‡] Benjamín J. Alemán,[†] Jonathan C. Lee,[§] Kenichi Ohno,[†] Charles F. de las Casas,[†,‡] F. Joseph Heremans,[†,‡] Evelyn L. Hu,[§] and David D. Awschalom*[,†,‡]

[†]Center for Spintronics and Quantum Computation, University of California, Santa Barbara, Santa Barbara, California 93106, United States

[‡]Institute for Molecular Engineering, University of Chicago, Chicago, Illinois 60637, United States

[§]School of Engineering and Applied Sciences, Harvard University, Cambridge, Massachusetts 02138, United States

Supporting Information

ABSTRACT: The nitrogen-vacancy (NV) center in diamond is an attractive platform for quantum information and sensing applications because of its room temperature operation and optical addressability. A major research effort focuses on improving the quantum coherence of this defect in engineered micro- and nanoscale diamond particles (DPs), which could prove useful for high-resolution sensing in fluidic environments. In this work we fabricate cylindrical diamonds particles with finely tuned and highly reproducible sizes (diameter and height ranging from 100 to 700 and 500 nm to 2 μm, respectively) using high-purity, single-crystal diamond membranes with shallow-doped NV centers. We show that the spin coherence time of the NV centers in these particles exceeds 700 μs, opening the possibility for the creation of ultrahigh sensitivity micro- and nanoscale sensors. Moreover, these particles can be efficiently transferred into a water suspension and delivered to the region to probe. In particular, we introduce a DP suspension inside a microfluidic circuit and control position and orientation of the particles using an optical trapping apparatus. We demonstrate a DC magnetic sensitivity of 9 $\mu T/\sqrt{Hz}$ in fluid as well as long-term trapping stability (>30 h), which paves the way toward the use of high-sensitivity pulse techniques on contactless probes manipulated within biological settings.

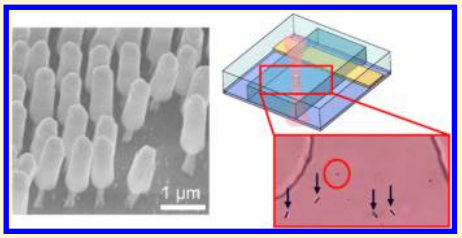

KEYWORDS: *Nanodiamond, microdiamond, nitrogen vacancy (NV) center, long spin coherence, nanoscale sensing, microfluidics, optical trapping*

The negatively charged nitrogen-vacancy (NV) center in diamond[1−4] has become a prominent room-temperature spin system for quantum information and sensing applications owing to its inherent optical addressability and long spin coherence times.[5−11] In particular, a major research effort has focused on exploiting the metrology capabilities of the NV center to investigate the details of biological systems at the nanoscale using diamond micro- and nanoparticles. These particles behave like highly localized, low-thermal-mass spin systems and can therefore be used for high spatial resolution, high-sensitivity mapping of their environment. For example, in recent years, micro- and nanoscale diamond particles (DPs) have been employed as biocompatible quantum probes in thermometry[12] and electromagnetic sensing[13] and have been integrated with atomic force microscopes[14] and optical tweezer platforms[15,16] to create NV center-based scanning probes. DPs have also been proposed for monitoring single ion channel activities in neurons[17] and sensing low-density magnetic impurities in a fluidic environment.[18]

One of the primary challenges inherent to using DPs as quantum probes is the marked degradation of the spin coherence of the NV centers within these structures relative to bulk diamond.[13,19−21] Improving the coherence properties in DPs has been a central research focus since they ultimately limit the achievable sensitivity. The lack of geometric control over the DPs' shape, size, and crystal orientation and the absence of an adequate means to engineer the position and density of the incorporated NV centers have further limited the practical use of DPs in sensing applications. The geometric factors, for example, compromise the stability and the orientation control of micro- and nanodiamonds optically trapped in aqueous environments,[15] hindering their sensing potential. Additionally, the control over the spatial distribution of the NV centers is critical to obtain single defects in proximity to the DP's surface, which is imperative for the sensing of single spins outside the diamond lattice.[22,23] These challenges have been partially addressed using multiple top-down techniques to fabricate DPs with controlled geometries both in polycrystalline and single crystal diamond.[24−26] Separately, relatively long NV center spin coherence has been observed using optimized dynamical decoupling pulse sequences in DPs with low densities of paramagnetic impurities.[27,28]

Received: April 1, 2014
Revised: July 24, 2014

dx.doi.org/10.1021/nl501208s | *Nano Lett.* XXXX, XXX, XXX−XXX

In this work, we implement a DP fabrication process that allows us to obtain NV centers with long spin coherence times that are embedded with controlled density and spatial distribution within single-crystal DPs. Our approach combines a high quality diamond epitaxial growth[29] with an established technique for diamond membrane fabrication,[30] along with electron beam lithography to pattern the DPs with a finely tuned shape and size. The use of diamond membranes is crucial to obtain an efficient release of the particles in suspension at the end of the fabrication process. Specifically, we fabricate cylindrical DPs (diameters ranging from 100 to 700 nm and lengths from 500 nm to 2 μm) incorporating single NV centers exhibiting consistently high Hahn echo coherence times ($T_{2,\mathrm{Hahn}}$ ~100 μs on average) up to ~360 μs. The coherence is further extended to ~710 μs using more advanced dynamical decoupling techniques. Additionally, we fabricate high-photoluminescence, high-aspect-ratio DPs and use them for optical trapping experiments inside of a microfluidic circuit. We show that the control over the particle's geometry is crucial in achieving long-term (over 30 h) trapping and orientation stability. These results pave the way for magnetic field and temperature mapping with bulk-like sensitivity in solution.

The fabrication process (described in detail in the Supporting Information) begins by creating a disordered layer in an electronic grade diamond substrate ([100] surface normal) using helium ion implantation (Figure 1a). We subsequently use plasma enhanced chemical vapor deposition (PECVD) to grow a diamond layer doped with ^{15}N (Figure 1b) to create isotopically tagged NV centers.[29,31] We use two separate growth recipes to obtain membranes with distinct NV center densities and properties. In one case (growth structure 1) we use a fast growth (~50 nm/min) combined with uniform ^{15}N doping of the PECVD diamond layer to obtain a large number of uniformly distributed NV centers in a thick (1.0−1.5 μm) membrane. The second type of growth (growth structure 2) is performed at a slower rate (~10 nm/h) to prevent structural defects and involves precisely timed ^{15}N doping. This recipe results in a ~6 nm thick NV center layer sandwiched between two ~100 nm high purity diamond layers (delta-doped membranes). Furthermore, this recipe utilizes an isotopically pure ^{12}C diamond lattice to create a nuclear spin-free environment conducive to high spin coherence times.[32] Next, the disordered layer is selectively electrochemically etched to release the newly grown membrane, which is then bonded (PECVD grown face down) to a carrier wafer using poly(methyl methacrylate) (PMMA), an easily employed and etchable transfer layer. The residual damaged layer of the electronic grade diamond plate is removed with a reactive ion etch (details of this process have been previously described[30]). Finally, we use electron beam lithography to define a hydrogen silsesquioxane (HSQ) hard mask array of circles with varying radii (Figure 1c). The hard mask protects the diamond during a subsequent oxygen inductively coupled plasma (ICP) etch, which transfers the mask pattern to the underlying diamond membrane to yield cylindrical DPs (Figure 1d). In Figure 1e, we show a scanning electron microscope (SEM) image of an array of particles patterned in a diamond membrane. By carefully controlling the etch time through the membrane, we obtain DPs attached to the substrate by a thin anchor of PMMA (Figure 1f), which facilitates the release and suspension of the particles in solvent.

We note that particles obtained from the uniformly doped material (growth structure 1) can be useful in applications

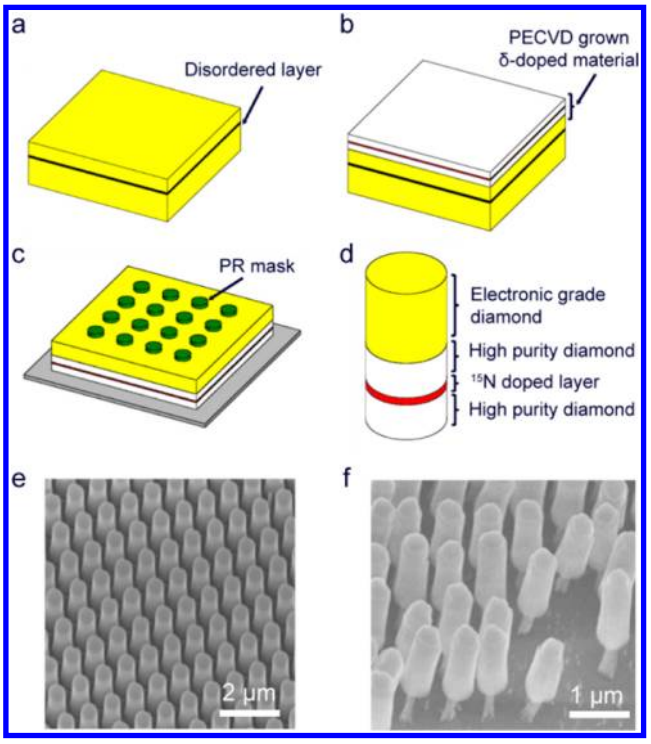

Figure 1. (a−d) Process flow schematics of the engineered diamond particle (DP) fabrication for the case of a delta-doped membrane. (a) Electronic-grade bulk diamond is implanted with helium ions (He^+) creating a disordered layer below the diamond surface (black layer). (b) Isotopically pure diamond (^{12}C) is grown on top of the He^+ implanted substrate using plasma enhanced chemical vapor deposition (PECVD). ^{15}N doped regions (red) can be introduced in between highly pure diamond layers (white) in a controlled way. Electron irradiation and annealing are used to promote the formation of NV centers at the nitrogen locations. (c) The disordered layer is electrochemically etched to release a thin diamond membrane, which is then transferred regrown-side down on a silicon substrate and bonded using photoresist. The membrane is further thinned using oxygen inductively coupled plasma (O_2-ICP) to remove the damaged diamond layer and obtained the desired membrane thickness. (d) An etch mask is patterned on the membrane by electron beam lithography. O_2-ICP transfers the mask pattern to the underlying membrane to form cylindrically shaped DPs. (e) Scanning electron microscope (SEM) image of an array of 500 nm diameter diamond particles, with 700 nm pitch and ~1 μm height. (f) Diamond particles anchored to the underlying substrate by a photoresist pillar. The particles are released in solution by sonication in water or by etching the resist anchor with solvent.

where it is important to have a high luminescence rate, such as in some temperature sensing schemes.[12] On the other hand, the delta-doped material (growth structure 2) is essential to fabricating particles containing a low density of NV centers with long spin coherence times in proximity of the diamond surface, required in applications such as high-sensitivity, high spatial resolution measurements of external spin species.

The DP photoluminescence (PL) and spin properties[3,4] are characterized before and after they are released from the substrate. We use a home-built confocal optical microscope apparatus[1] to initialize and read out the NV centers' spin states and a microwave antenna to drive spin transitions.[33] Figure 2a shows a scanning confocal optical image of an array of 300 nm diameter particles from a delta-doped membrane. We found that, as expected,[34] we can modify the intensity of the PL

dx.doi.org/10.1021/nl501208s | Nano Lett. XXXX, XXX, XXX−XXX

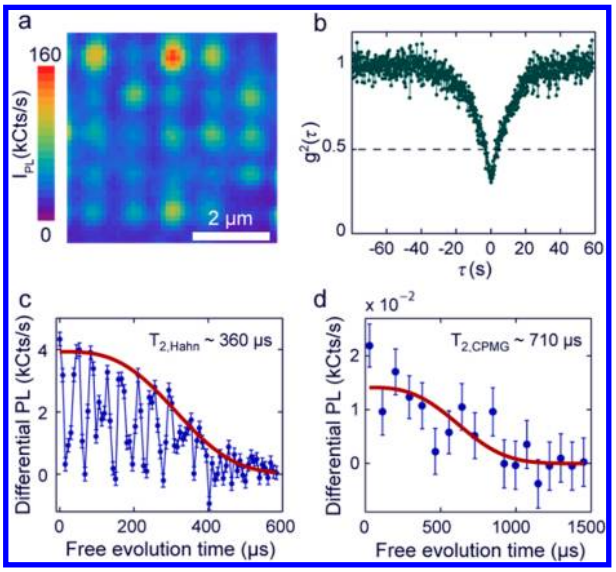

Figure 2. (a) Scanning optical confocal image of an array of 300 nm diameter diamond particles. (b) Photon correlation curve obtained from a single NV center particle showing antibunching ($g^2(0) < 0.5$). (c) Hahn-echo measurement obtained on a particle incorporating a single NV center. We fit the envelope of the data to $Ae^{-(t/T_2)^3}$ (see the Supporting Information for details) and extract a coherence time of $T_{2,Hahn} = 357 \pm 38$ μs. (d) CPMG measurement obtained on the same particle using a sequence of five π-pulses. A fit of the data analogous to the one used for the Hahn echo curve gives us $T_{2,CPMG} = 708 \pm 215$ μs. All of the uncertainties are quoted at 95% confidence.

collected from the DPs by tuning their diameter, due to variations in the photon collection efficiency. In particular, we observed a nearly 10-fold signal increase in the 220 nm diameter particles compared to the signal coming from the unprocessed membrane (see the Supporting Information).

To show that our fabrication process is suitable to access the single defect regime, we collect photon correlation curves using a standard Hanbury-Brown and Twiss measurement scheme. In Figure 2c, we show the correlation curve (with no background correction) for a 300 nm diameter DP incorporating a single NV center, demonstrating strong photon antibunching ($g^{(2)}(0) < 0.5$). Using the PL intensity collected for a single NV as a reference and correcting for the variations in the collection efficiencies, we estimate that the NV center density varies between 0 and 10 NV centers per particle across the different particle sizes. We confirmed that we are addressing engineered NV centers, rather than those native to the bulk diamond, by showing that the hyperfine structure of high resolution optically detected magnetic resonance (ODMR) spectra is consistent with ^{15}N hyperfine interaction (see the Supporting Information).

The spin coherence of the NV centers is inferred from the decay time of coherence curves obtained with standard Hahn echo measurements ($T_{2,Hahn}$). We first focus on the analysis of the delta-doped material (growth structure 2). Initially, we inspect the coherence time of the NV centers in an unprocessed delta-doped membrane to ensure that the membrane preparation process leaves the NV centers' properties intact. Two separate measurements (not shown) give us $T_{2,Hahn} \sim 305$ μs and ~750 μs, respectively, in line with what is expected for NV centers ~100 nm below the surface of isotopically pure, delta-doped bulk diamond.[29] We then measured $T_{2,Hahn}$ for a series of particles. The selected DPs have diameters of 300 and 500 nm and contain single NV centers. The average $T_{2,Hahn}$ decreases to ~100 μs though some values (3 out of 10) are in excess of 200 μs, with a highest value of 357 ± 38 μs (Figure 2d). The oscillations in the Hahn-echo curves are associated with the interaction of the NV center's electronic spin with both the ^{15}N nuclear spin comprising the NV center and the ^{15}N spin bath surrounding the defect (see details in the Supporting Information). The broad distribution of $T_{2,Hahn}$ values is likely associated with variations in the position of the NV centers with respect to the DPs' sidewalls, as proximity to the diamond surface deteriorates the NV center coherence.[29,35] Because of this effect, a direct comparison of the spin coherence with previous results[27,28] would require a full analysis of the NV center's exact position with respect to the surface of the DPs. Nevertheless, we emphasize that, thanks to the high thermal conductivity of diamond, the distance of the NV center from the sidewalls is irrelevant to temperature sensing purposes in particles this size.

In order to estimate the full potential of our DPs, we also collect coherence measurements using a single axis Carr−Purcell−Meiboom−Gill (CPMG) sequence composed of five π-pulses (see the Supporting Information for details). With this approach we are able to extend the coherence time up to $T_{2,CPMG} = 708 \pm 215$ μs (Figure 2d). All uncertainties are quoted at 95% confidence. The CPMG data also show evidence of the ^{15}N related oscillations due to the sampling rate of the full trace. These partial oscillations complicate the fit of the data, resulting in the large uncertainty we report. We emphasize that replacing ^{15}N doping with ^{14}N doping would eliminate the oscillations in the signal[36] and simplify the data analysis.

For comparison, we also analyze the properties of DPs obtained from a uniformly doped membrane (growth structure 1). Continuous wave (CW) ODMR spectra show four pairs of peaks for a randomly oriented external magnetic field (see the Supporting Information), consistent with the expected distribution of NV centers in all four crystal orientations for a single-crystal diamond sample. The single-crystal nature of the engineered particles was confirmed by transmission electron microscopy (TEM, see the Supporting Information.). The $T_{2,Hahn}$ times are typically shorter (<5 μs) both for the bulk membranes and for the particles, due to the decoherence effects of ^{13}C atoms and of structural defects present in the rapidly grown material.

To demonstrate the suitability of our engineered DPs as contactless scanning micro- and nanoprobes, we use them to perform high-sensitivity measurements in aqueous solutions, in combination with an optical tweezers apparatus.[15] As a proof-of-concept, we work with high PL particles obtained from the uniformly doped material (growth structure 1) in order to obtain a larger signal-to-noise ratio. When working with commercial DPs, a small size (≤100 nm) is necessary to have well-localized NV centers that are close to the particle surface. However, particles this size are considerably smaller than the trapping volume (~1.5 μm^3) determined by the beam waist and Rayleigh length of the focused trapping laser. Therefore, many DPs can simultaneously occupy the trap, resulting in complex dynamics in the trapped region. Furthermore, over the course of a single measurement, many particles may enter or exit the trap, leading to large fluctuations in the emitted fluorescence. These effects preclude experiments on single particles that require long-term stability (e.g., pulse sequence measurements) and result in a degradation of the signal-to-noise ratio. We address these stability issues with a 2-fold approach. First, we

dx.doi.org/10.1021/nl501208s | Nano Lett. XXXX, XXX, XXX−XXX

trap ~500 nm diameter, ~2 μm long DPs, which occupy most of the trapping volume, strongly reducing the chances of multiple trapping. Additionally, we engineer a polydimethylsiloxane (PDMS) microfluidic circuit[37] and integrate it with the optical tweezers apparatus (Figure 3a). This circuit allows us to

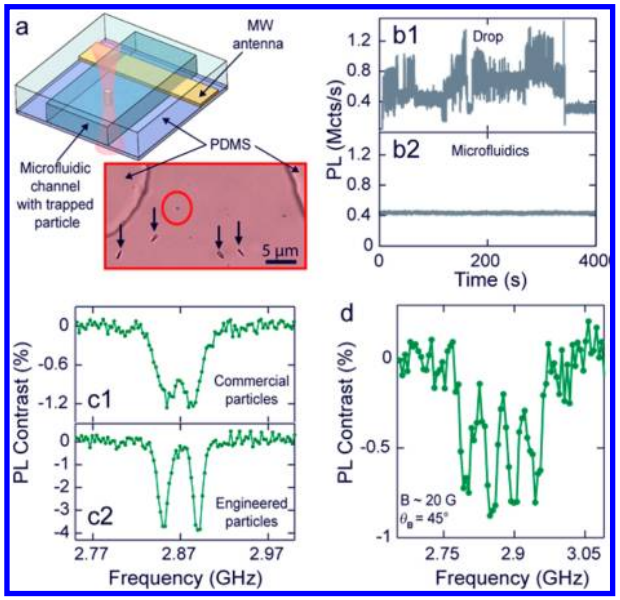

Figure 3. (a) Sketch of the optical tweezers/microfluidic apparatus around the trap region. The infrared trapping laser and the green probe laser are focused via a microscope objective (not shown) inside a microfluidic channel created in a PDMS layer bonded on top of a glass slide. A coplanar waveguide is patterned on the glass slide for microwave generation. Inset: CCD camera picture of the interior of the microfluidic channel with a solution of engineered DPs. Some DPs stuck to the bottom of the channel are indicated by arrows. One particle is trapped along its axis and levitated (red circle). (b1) Time trace of the photoluminescence signal collected from commercial DPs trapped in a drop of solution deposited on a bare glass slide and (b2) flowed inside the fabricated microfluidic channel (bottom). (c1) CW-ODMR spectra of commercial DPs and (c2) of an engineered DP optically trapped in a microfluidic circuit. An external magnetic field (~10 G) is applied along the axis of the trap (54.7° with respect to the NV centers orientations). The signal is averaged for 0.6 s at each frequency point. (d) CW-ODMR spectra of an optically trapped engineered DP in the presence of a magnetic field (~20 G) applied at ~45° with respect to the trap axis. The signal was averaged for two seconds at each frequency point.

efficiently transport a suspension of DPs into the trap region and, once a single particle is trapped, to flow deionized water to flush out excess particles and obtain a well-controlled surrounding environment. In Figure 3b1, we report a time trace of the PL signal coming from commercial DPs (ND-NV-100 nm, Adámas Nanotechnology) optically trapped in a drop of suspension deposited on a bare glass slide, which clearly shows PL instability. In Figure 3b2, we show the PL trace for commercial DPs trapped inside our microfluidic circuit. Both traces are plotted using the same vertical scale to highlight the improvement in the signal stability. Specifically, the standard deviations of the PL signal in the droplet and in the microfluidic channel are respectively ~238 kCts/s and ~9 kCts/s.

Another important limitation of commercial particles is associated with their random shape, which prevents a priori determination of the NV center orientations and results in uncontrolled rotational motion in aqueous environments. Random rotational dynamics complicate the interpretation of sensing measurements[15] and ultimately limit the use of dynamical decoupling techniques.

In Figure 3c1, we show a CW-ODMR spectrum for a group of commercial DPs trapped inside a microfluidic channel in the presence of an external constant and uniform magnetic field (B ~ 10 G) aligned along the trap axis (traveling axis of the trapping laser). We find that, even in a well-controlled environment, the effect of the rotation dynamics is evident and results in a spectrum with two broad peaks having a full-width-half-max (fwhm) of ~30 MHz. In contrast, by carefully designing the geometry of our engineered particles, we introduce a preferential axis along which the DPs' main axis (parallel to the [100] crystal lattice as confirmed by TEM measurements) tend to align within the trap.[38,39] For our experiment, this preferential axis is the same as the trap axis. In the inset of Figure 3a we show a picture of the interior of a microfluidic circuit around the optical trap region. The particles indicated with arrows are stuck to the bottom of the microfluidic channel. In the center, we highlight a particle that is levitated with the optical tweezers' infrared laser and appears upright, with its main axis along the optical trap axis. In Figure 3c2, we show the CW-ODMR spectrum we collect for a magnetic field (B ~ 10 G) applied along the axis of the trap. Two well-separated peaks are visible, as expected for a cylindrical particle with [100] axis aligned along the magnetic field, as the four possible NV center orientations are degenerate with respect to the magnetic field orientation. The fwhm of the peaks is ~10 MHz, similar to what has previously been obtained with CW-ODMR measurements both of ensembles of NV centers in bulk diamond[40] and of single NV centers in DPs attached to an AFM tip.[14] This result further suggests that the particle is indeed trapped along the crystal axis and that this axis is not appreciably precessing during the 400 s measurement.

To gain further insights in the trapped particle dynamics, we collect CW-ODMR spectra with a magnetic field tilted with respect to the trap axis. In these conditions, we expect to see anywhere between two and four distinct peak pairs in the spectrum if the particle is not revolving around its main axis. In Figure 3d, we show the result obtained with a magnetic field of ~20 G applied at ~45° from the trap axis, where four distinct peaks are visible. Their fwhm (~25 MHz) and the spectra collected at higher magnetic fields (see the Supporting Information) both suggest that each peak is actually a convolution of two peaks. The ability to resolve the CW-ODMR spectrum structure suggests that the trapped particle does not noticeably revolve around its main axis during the time it takes to perform the measurement (800 s). We emphasize that we were able to trap particles for up to 30 h before purposely releasing them, which serves as another indication of the good stability of the system.

These results are important advancements toward using optically trapped diamond particles as magnetic field and temperature sensors. From a series of CW-ODMR measurements collected at different magnetic fields (see the Supporting Information), we estimate an experimental DC magnetic field sensitivity of ~9 $\mu T/\sqrt{Hz}$, but this sensitivity could be further enhanced by employing pulsed techniques to avoid power broadening in the CW-ODMR spectrum and by using isotopically pure material for the growth. We indeed observe an increase in T_2^* (the meaningful parameter for DC magnetometry applications[41]) from a few hundred nanoseconds, in the nanoparticles obtained from growth structure

dx.doi.org/10.1021/nl501208s | Nano Lett. XXXX, XXX, XXX−XXX

1, up to 6.42 ± 1.05 μs, in the ones fabricated with the isotopically pure material (see the Supporting Information). Additionally, the use of a pulsed optical trap would reduce the detrimental effect of the infrared laser on the NV centers' PL,[42] increasing the signal-to-noise ratio of the measurements.

In this work, we engineered single-crystal cylindrical micro- and nanoscale diamond particles with a reproducible shape, size, and crystal orientation. Crucially, the DPs can efficiently be released from the substrate and dispersed in solvent. Using high-quality, delta-doped diamond membranes, we are able to obtain DPs containing single NV centers with long coherence times ($T_{2,\mathrm{CPMG}}$ up to 710 μs). These particles should prove useful as high-sensitivity, high spatial resolution probes and as a source of confined quantum systems that can be integrated with photonics and optomechanical devices. A possible approach to improve the potential of these DPs would be to combine our fabrication process with a technique to obtain lateral positioning of the NV centers relative to the sidewalls. This would enable the creation of particles incorporating NV centers with long, highly predictable spin coherence times and well-known distance from the diamond surface, which are critical parameters to interpreting the magnetic signature of external spins. We also fabricate DPs with a high number of NV centers and use them in combination with an optical tweezers apparatus. When integrated with a microfluidic environment, this approach allows us to stably and steadily trap our DPs and perform CW-ODMR measurements for more than 30 h. This stability is the result of the carefully engineered shape of the DPs. Using the system as a DC magnetometer, we demonstrate a magnetic field sensitivity of $\sim 9\ \mu\mathrm{T}/\sqrt{\mathrm{Hz}}$, which is comparable to the typical values for immobilized diamond structures.[43] Furthermore, these results suggest that our optically trapped DPs are sufficiently stable to be easily used in combination with dynamical decoupling techniques and could lead to the realization of low-thermal-mass, high-sensitivity probes for fluctuating magnetic field and temperatures[44,45] in fluid. For instance, our DPs could be used to determine important parameters in microfluidic environments such as the temperature of chemical reactions, or they could be manipulated inside a biological environment to explore the details of these systems at the nanoscale.

■ ASSOCIATED CONTENT

Supporting Information

Details of the diamond particle fabrication process. Transmission electron microscopy analysis of the DPs. Analysis of the particles' collection efficiency. Description of the measurements used to achieve nitrogen isotope discrimination and to obtain the spin coherence evolution curves. CW-ODMR spectra of high PL DPs in the presence of an external magnetic field. Analysis of the DC magnetic field sensitivity. This material is available free of charge via the Internet at http://pubs.acs.org.

■ AUTHOR INFORMATION

Corresponding Author

*E-mail address: awsch@uchicago.edu.

Present Address

B.J.A.: Department of Physics, University of Oregon, Eugene, OR 97403, United States.

Author Contributions

P.A. and B.J.A. contributed equally.

Notes

The authors declare no competing financial interest.

■ ACKNOWLEDGMENTS

The authors would like to thank V. R. Horowitz for previous work on the apparatus, A. N. Cleland for valuable discussions, C. A. McLellan for assistance with the diamond growth, and S. Kraemer for assistance with the TEM. We acknowledge the support of the California Nanosystems Institute. A portion of this work was done in the University of California Santa Barbara Nanofabrication facility, part of the National Science Foundation-funded National Nanotechnology Infrastructure Network. We acknowledge financial support from DARPA, AFOSR, and the DIAMANT program. B.J.A. acknowledges support from the University of California President's Postdoctoral Fellowship.

■ REFERENCES

(1) Gruber, A.; Dräbenstedt, C.; Tietz, L.; Fleury, J.; Wrachtrup; von Borczyskowski, C. Scanning Confocal Optical Microscopy and Magnetic Resonance on Single Defect Centers. *Science* **1997**, *276*, 2012−2014.

(2) Manson, N. B.; Harrison, J. P.; Sellars, M. J. Nitrogen-Vacancy Center in Diamond: Model of the Electronic Structure and Associated Dynamics. *Phys. Rev. B* **2006**, *74*, 104303.

(3) Dobrovitski, V. V.; Fuchs, G. D.; Falk, A. L.; Santori, C.; Awschalom, D. D. Quantum Control Over Single Spins in Diamond. *Annu. Rev. Condens. Matter Phys.* **2013**, *4*, 7.1−7.28.

(4) Doherty, M. W.; Manson, N. B.; Delaney, P.; Jelezko, F.; Wrachtrup, J.; Hollenberg, L. C. L. The Nitrogen-Vacancy Colour Centre in Diamond. *Phys. Rep.* **2013**, *528*, 1−45.

(5) Dolde, F.; Fedder, H.; Doherty, M. W.; Nöbauer, T.; Rempp, F.; Balasubramanian, G.; Wolf, T.; Reinhard, F.; Hollenberg, L. C. L.; Jelezko, F.; et al. Electric-Field Sensing Using Single Diamond Spins. *Nat. Phys.* **2011**, *7*, 459−463.

(6) Balasubramanian, G.; Chan, I. Y.; Kolesov, R.; Al-Hmoud, M.; Tisler, J.; Shin, C.; Kim, C.; Wojcik, A.; Hemmer, P. R.; Krueger, A.; et al. Nanoscale Imaging Magnetometry with Diamond Spins under Ambient Conditions. *Nature* **2008**, *455*, 648−651.

(7) Toyli, D. M.; de Las Casas, C. F.; Christle, D. J.; Dobrovitski, V. V.; Awschalom, D. D. Fluorescence Thermometry Enhanced by the Quantum Coherence of Single Spins in Diamond. *Proc. Natl. Acad. Sci. U.S.A.* **2013**, *110*, 8417−8421.

(8) Neumann, P.; Jakobi, I.; Dolde, F.; Burk, C.; Reuter, R.; Waldherr, G.; Honert, J.; Wolf, T.; Brunner, A.; Shim, J. H.; et al. High-Precision Nanoscale Temperature Sensing Using Single Defects in Diamond. *Nano Lett.* **2013**, *13*, 2738−2742.

(9) Wrachtrup, J.; Jelezko, F. Processing Quantum Information in Diamond. *J. Phys.: Condens. Matter* **2006**, *18*, S807−S824.

(10) Fuchs, G. D.; Burkard, G.; Klimov, P. V.; Awschalom, D. D. A Quantum Memory Intrinsic to Single Nitrogen−vacancy Centres in Diamond. *Nat. Phys.* **2011**, *7*, 789−793.

(11) Toyli, D.; Christle, D.; Alkauskas, A.; Buckley, B.; Van de Walle, C.; Awschalom, D. D. Measurement and Control of Single Nitrogen-Vacancy Center Spins above 600 K. *Phys. Rev. X* **2012**, *2*, 1−7.

(12) Kucsko, G.; Maurer, P. C.; Yao, N. Y.; Kubo, M.; Noh, H. J.; Lo, P. K.; Park, H.; Lukin, M. D. Nanometre-Scale Thermometry in a Living Cell. *Nature* **2013**, *500*, 54−58.

(13) McGuinness, L. P.; Yan, Y.; Stacey, A.; Simpson, D. A.; Hall, L. T.; Maclaurin, D.; Prawer, S.; Mulvaney, P.; Wrachtrup, J.; Caruso, F.; et al. Quantum Measurement and Orientation Tracking of Fluorescent Nanodiamonds inside Living Cells. *Nat. Nanotechnol.* **2011**, *6*, 358−363.

(14) Rondin, L.; Tetienne, J.-P.; Spinicelli, P.; Dal Savio, C.; Karrai, K.; Dantelle, G.; Thiaville, A.; Rohart, S.; Roch, J.-F.; Jacques, V. Nanoscale Magnetic Field Mapping with a Single Spin Scanning Probe Magnetometer. *Appl. Phys. Lett.* **2012**, *100*, 153118.

(15) Horowitz, V. R.; Alemán, B. J.; Christle, D. J.; Cleland, A. N.; Awschalom, D. D. Electron Spin Resonance of Nitrogen-Vacancy Centers in Optically Trapped Nanodiamonds. *Proc. Natl. Acad. Sci. U.S.A.* **2012**, *109*, 13493−13497.
(16) Geiselmann, M.; Juan, M. L.; Renger, J.; Say, J. M.; Brown, L. J.; de Abajo, F. J. G.; Koppens, F.; Quidant, R. Three-Dimensional Optical Manipulation of a Single Electron Spin. *Nat. Nanotechnol.* **2013**, 1−5.
(17) Hall, L. T.; Hill, C. D.; Cole, J. H.; Städler, B.; Caruso, F.; Mulvaney, P.; Wrachtrup, J.; Hollenberg, L. C. L. Monitoring Ion-Channel Function in Real Time through Quantum Decoherence. *Proc. Natl. Acad. Sci. U.S.A.* **2010**, *107*, 18777−18782.
(18) Steinert, S.; Ziem, F.; Hall, L. T.; Zappe, a.; Schweikert, M.; Götz, N.; Aird, a.; Balasubramanian, G.; Hollenberg, L.; Wrachtrup, J. Magnetic Spin Imaging under Ambient Conditions with Sub-Cellular Resolution. *Nat. Commun.* **2013**, *4*, 1607.
(19) Laraoui, A.; Hodges, J. S.; Meriles, C. A. Nitrogen-Vacancy-Assisted Magnetometry of Paramagnetic Centers in an Individual Diamond Nanocrystal. *Nano Lett.* **2012**, *12*, 3477−3482.
(20) Tisler, J.; Balasubramanian, G.; Naydenov, B.; Kolesov, R.; Grotz, B.; Reuter, R.; Boudou, J.-P.; Curmi, P. A.; Sennour, M.; Thorel, A.; et al. Fluorescence and Spin Properties of Defects in Single Digit Nanodiamonds. *ACS Nano* **2009**, *3*, 1959−1965.
(21) Rabeau, J. R.; Stacey, A.; Rabeau, A.; Prawer, S.; Jelezko, F.; Mirza, I.; Wrachtrup, J. Single Nitrogen Vacancy Centers in Chemical Vapor Deposited Diamond Nanocrystals. *Nano Lett.* **2007**, *7*, 3433−3437.
(22) Mamin, H. J.; Sherwood, M. H.; Rugar, D. Detecting External Electron Spins Using Nitrogen-Vacancy Centers. *Phys. Rev. B* **2012**, *86*, 195422.
(23) Mamin, H. J.; Kim, M.; Sherwood, M. H.; Rettner, C. T.; Ohno, K.; Awschalom, D. D.; Rugar, D. Nanoscale Nuclear Magnetic Resonance with a Nitrogen-Vacancy Spin Sensor. *Science* **2013**, *339*, 557−560.
(24) Hausmann, B. J. M.; Khan, M.; Zhang, Y.; Babinec, T. M.; Martinick, K.; McCutcheon, M.; Hemmer, P. R.; Lončar, M. Fabrication of Diamond Nanowires for Quantum Information Processing Applications. *Diam. Relat. Mater.* **2010**, *19*, 621−629.
(25) Evtimova, J.; Kulisch, W.; Petkov, C.; Petkov, E.; Schnabel, F.; Reithmaier, J. P.; Popov, C. Reactive Ion Etching of Nanocrystalline Diamond for the Fabrication of One-Dimensional Nanopillars. *Diam. Relat. Mater.* **2013**, *36*, 58−63.
(26) Petkov, E.; Popov, C.; Rendler, T.; Petkov, C.; Schnabel, F.; Fedder, H.; Lee, S.-Y.; Kulisch, W.; Reithmaier, J. P.; Wrachtrup, J. Investigation of NV Centers in Diamond Nanocrystallites and Nanopillars. *Phys. Status Solidi* **2013**, *250*, 48−50.
(27) Trusheim, M. E.; Li, L.; Laraoui, A.; Chen, E. H.; Bakhru, H.; Schröder, T.; Gaathon, O.; Meriles, C. A.; Englund, D. Scalable Fabrication of High Purity Diamond Nanocrystals with Long-Spin-Coherence Nitrogen Vacancy Centers. *Nano Lett.* **2014**, *14*, 32−36.
(28) Knowles, H. S.; Kara, D. M.; Atatüre, M. Observing Bulk Diamond Spin Coherence in High-Purity Nanodiamonds. *Nat. Mater.* **2014**, *13*, 21−25.
(29) Ohno, K.; Heremans, F. J.; Bassett, L. C.; Myers, B. A.; Toyli, D. M.; Jayich, A. C. B.; Palmstrøm, C. J.; Awschalom, D. D. Engineering Shallow Spins in Diamond with Nitrogen Delta-Doping. *Appl. Phys. Lett.* **2012**, *101*, 082413.
(30) Magyar, A. P.; Lee, J. C.; Limarga, A. M.; Aharonovich, I.; Rol, F.; Clarke, D. R.; Huang, M.; Hu, E. L. Fabrication of Thin, Luminescent, Single-Crystal Diamond Membranes. *Appl. Phys. Lett.* **2011**, *99*, 081913.
(31) Rabeau, J. R.; Reichart, P.; Tamanyan, G.; Jamieson, D. N.; Prawer, S.; Jelezko, F.; Gaebel, T.; Popa, I.; Domhan, M.; Wrachtrup, J. Implantation of Labelled Single Nitrogen Vacancy Centers in Diamond Using ^{15}N. *Appl. Phys. Lett.* **2006**, *88*, 023113.
(32) Balasubramanian, G.; Neumann, P.; Twitchen, D.; Markham, M.; Kolesov, R.; Mizuochi, N.; Isoya, J.; Achard, J.; Beck, J.; Tissler, J.; et al. Ultralong Spin Coherence Time in Isotopically Engineered Diamond. *Nat. Mater.* **2009**, *8*, 383−387.
(33) Jelezko, F.; Gaebel, T.; Popa, I.; Gruber, A.; Wrachtrup, J. Observation of Coherent Oscillations in a Single Electron Spin. *Phys. Rev. Lett.* **2004**, *92*, 076401.
(34) Babinec, T. M.; Hausmann, B. J. M.; Khan, M.; Zhang, Y.; Maze, J. R.; Hemmer, P. R.; Lončar, M. A Diamond Nanowire Single-Photon Source. *Nat. Nanotechnol.* **2010**, *5*, 195−199.
(35) Myers, B. A.; Das, A.; Dartiailh, M. C.; Ohno, K.; Awschalom, D. D.; Jayich, A. C. B. Probing Surface Noise with Depth-Calibrated Spins in Diamond. *Phys. Rev. Lett.* **2014**, *113*, 027602.
(36) Childress, L.; Gurudev Dutt, M. V.; Taylor, J. M.; Zibrov, A. S.; Jelezko, F.; Wrachtrup, J.; Hemmer, P. R.; Lukin, M. D. Coherent Dynamics of Coupled Electron and Nuclear Spin Qubits in Diamond. *Science* **2006**, *314*, 281−285.
(37) Mcdonald, J. C.; Duffy, D. C.; Anderson, J. R.; Chiu, D. T.; Wu, H.; Schueller, O. J. A.; Whitesides, G. M. Fabrication of Microfluidic Systems in Poly(dimethylsiloxane). *Electrophoresis* **2000**, *21*, 27−40.
(38) Cao, Y.; Stilgoe, A. B.; Chen, L.; Nieminen, T. A.; Rubinsztein-Dunlop, H. Equilibrium Orientations and Positions of Non-Spherical Particles in Optical Traps. *Opt. Express* **2012**, *20*, 12987−12996.
(39) Bareil, P. B.; Sheng, Y. Angular and Position Stability of a Nanorod Trapped in an Optical Tweezers. *Opt. Express* **2010**, *18*, 26388−26398.
(40) Acosta, V.; Bauch, E.; Ledbetter, M.; Santori, C.; Fu, K.-M.; Barclay, P.; Beausoleil, R.; Linget, H.; Roch, J.; Treussart, F.; et al. Diamonds with a High Density of Nitrogen-Vacancy Centers for Magnetometry Applications. *Phys. Rev. B* **2009**, *80*, 115202.
(41) Taylor, J. M.; Cappellaro, P.; Childress, L.; Jiang, L.; Budker, D.; Hemmer, P. R.; Yacoby, a.; Walsworth, R.; Lukin, M. D. High-Sensitivity Diamond Magnetometer with Nanoscale Resolution. *Nat. Phys.* **2008**, *4*, 810−816.
(42) Lai, N. D.; Faklaris, O.; Zheng, D.; Jacques, V.; Chang, H.-C.; Roch, J.-F.; Treussart, F. Quenching Nitrogen−vacancy Center Photoluminescence with an Infrared Pulsed Laser. *New J. Phys.* **2013**, *15*, 033030.
(43) Grinolds, M. S.; Hong, S.; Maletinsky, P.; Luan, L.; Lukin, M. D.; Walsworth, R. L.; Yacoby, a. Nanoscale Magnetic Imaging of a Single Electron Spin under Ambient Conditions. *Nat. Phys.* **2013**, *9*, 215−219.
(44) McGuinness, L. P.; Hall, L. T.; Stacey, A.; Simpson, D. A.; Hill, C. D.; Cole, J. H.; Ganesan, K.; Gibson, B. C.; Prawer, S.; Mulvaney, P.; et al. Ambient Nanoscale Sensing with Single Spins Using Quantum Decoherence. *New J. Phys.* **2013**, *15*, 073042.
(45) Hall, L. T.; Cole, J. H.; Hill, C. D.; Hollenberg, L. C. L. Sensing of Fluctuating Nanoscale Magnetic Fields Using NV Centres in Diamond. *Phys. Rev. Lett.* **2009**, *103*, 220802.